Fabrication of Solid Oxide Fuel Cells

and the Effects of Linear Siloxane Deposition on Cell Performance

by

Derall M. Riley

A Thesis Presented in Partial Fulfillment
of the Requirements for the Degree
Master of Science

Approved November 2021 by the
Graduate Supervisory Committee:

Ryan J. Milcarek, Chair
Patrick Phelan
Liping Wang

ARIZONA STATE UNIVERSITY

December 2021

ABSTRACT

Biogas's potential as a renewable fuel source has been an area of increased research in recent years. One issue preventing wide-spread use of biogas as a fuel is the trace amounts of impurities that damage fuel-burning equipment by depositing silicon, sulfur, calcium and other elements on their surface. This study aims to analyze the effects of a high concentration of L4 linear siloxane on solid oxide fuel cell performance until failure occurs. L4 siloxane has not been extensively researched previously, and this investigation aims to provide new data to support similar, though slower, degradation compared to D4, D5 and other siloxanes in solid oxide fuel cells. The experiments were conducted inside a furnace heated to 800°C with an Ni-YSZ-supported (Nickel-yttria-stabilized zirconia) fuel cell. A fuel source with a flow rate of 20 mL/min of hydrogen gas, 10 mL/min of nitrogen gas and 0.15 mL/min of L4 siloxane was used. Air was supplied to the cathode. The effects of siloxane deposition on cell voltage and power density degradation and resistance increase were studied by using techniques like the current-voltage method, electrochemical impedance spectroscopy, and gas chromatography. The results of the experiment after reduction show roughly constant degradation of 8.35 mV/hr, followed after approximately 8 hours by an increasing degradation until cell failure of 130.45 mV/hr. The initial degradation and stagnation match previous research in siloxane deposition on SOFCs, but the sharp decline to failure does not. A mechanism for solid oxide fuel cell failure is proposed based on the data.

ACKNOWLEDGEMENTS

I would like to thank Dr. Ryan Milcarek for the opportunity to work on this thesis project, and for his advice, many, many meetings, and words of encouragement throughout this entire process. I would also like to thank Dr. Patrick Phelan and Dr. Liping Wang for being willing to serve as thesis committee members for me. I also absolutely need to thank Jiashen Tian: the time he spent with me getting this project running, the help setting up the experimental set up and measuring equipment, the knowledge on combustion and SOFC experiments, and for helping me build this project into what it is.

TABLE OF CONTENTS

Page

CHAPTER Page

Page

APPENDIX

LIST OF TABLES

Table Page

LIST OF FIGURES

Figure Page

Figure Page

1. INTRODUCTION

In both landfills and wastewater treatment plants (WWTPs), biogas is created as a byproduct. In landfills, natural organic decomposition creates this gas, while in WWTPs, sludge that is filtered out of the process from clarifiers is piped into an anaerobic digester, where micro-organisms convert that sludge into biogas in an oxygen-deficient environment. This biogas in both landfills and wastewater treatment plants is a methane-dominant gaseous mixture, also consisting of carbon dioxide, nitrogen, and trace amounts of impurities like hydrogen sulfide, water, and various siloxanes. Biogas from WWTPs is roughly 55-65% methane (CH_4), with 35-45% carbon dioxide (CO_2) and trace amount of these impurities [1] while biogas from landfills is closer to 50% CH_4, 45% CO_2 and roughly 5% nitrogen (N_2) and other gases and impurities [2]. Because of the high methane content, biogas has the potential to be utilized as a fuel source in heating and power-generating processes, as its calorific value sits between 19.7 and 23.3 MJ/m^3 [1]. This is lower than that of natural gas's average heating value in the United States (roughly 38.6 MJ/m^3 in 2020) [3], but is still significant.

One downside to using biogas as a fuel source is the trace amounts of impurities. Sulfides, siloxanes, calcium, water and other impurities can all lead to deposition on equipment, which can lead to reduced performance and reduced equipment lifespan. Prime movers are typically used in conjunction with biogas to convert its chemical energy into a useable work, but all are susceptible to this deposition. Internal combustion engines, gas turbines, micro-turbines and Stirling engines are currently being utilized commonly as prime movers with biogas as a fuel source [4]. However, one alternative that is increasing

in popularity and feasibility are fuel cells, and specifically solid oxide fuel cells (SOFCs). Like other prime movers, SOFCs are susceptible to reduced life and performance from siloxane and sulfide buildup.

SOFCs operate similarly to other fuel cells, but must operate at higher temperatures due to their ceramic oxide electrolyte. Their usage as a prime mover in WWTPs, and the effects of siloxanes on cell performance has only begun being researched in the last two decades [5]. Nickel-based anodes with the cyclic D4 siloxane have been studied the most thoroughly [6–8], as D4 siloxane is the most common siloxane associated with biogas from WWTPs. Nickel anodes are utilized as nickel is widely commercially available, inexpensive, and the nickel acts as an electrocatalyst for hydrogen oxidation so no additional electrocatalyst is required [9,10].

While several studies on the effects of cyclic siloxanes like D4 on SOFC degradation have been completed, only one has been done on linear siloxanes like L3 and L4 [11]. Linear siloxanes typically appear at significantly lower concentrations than D3, D4, and D5 cyclic siloxanes in both landfill and wastewater biogas [12,13]. Tian and Milcarek did recently compare the effects of D4 and L4 siloxane on SOFC degradation and determined that L4 siloxanes showed lower degradation rates in SOFC performance, and showed less siloxane deposition on the surface of the anode [11].

2. LITERATURE REVIEW

This section includes the literature review for this thesis project, which provides background on the problem being addressed. This review will begin with an introduction into SOFCs: how they operate, and current usage, followed by a section on various fabrication techniques for SOFCs, and their strengths and weaknesses. Following this SOFC review, a review on various siloxanes will be presented, including where they are found, how they are formed, and their chemical compositions. Their usage and applications with SOFCs will then be addressed, as well as the degradation issues that plague SOFCs when a fuel source with siloxanes is utilized.

Solid Oxide Fuel Cells

Fuel cells are an electricity-producing device that use chemical energy via electrochemical reactions between elements from a fuel source and oxidant to produce power. Like a standard battery, fuel cells typically consist of two porous electrodes (one positive: the cathode, and one negative: the anode) split by an electrolyte. An external circuit connects the anode to the cathode and allows the flow of electrons from the anode to the cathode. A fuel source containing hydrogen molecules is fed to the anode side while an oxidant is fed to the cathode side. Figure 1 shows this set up and the electrochemical reactions associated with the fuel cell.

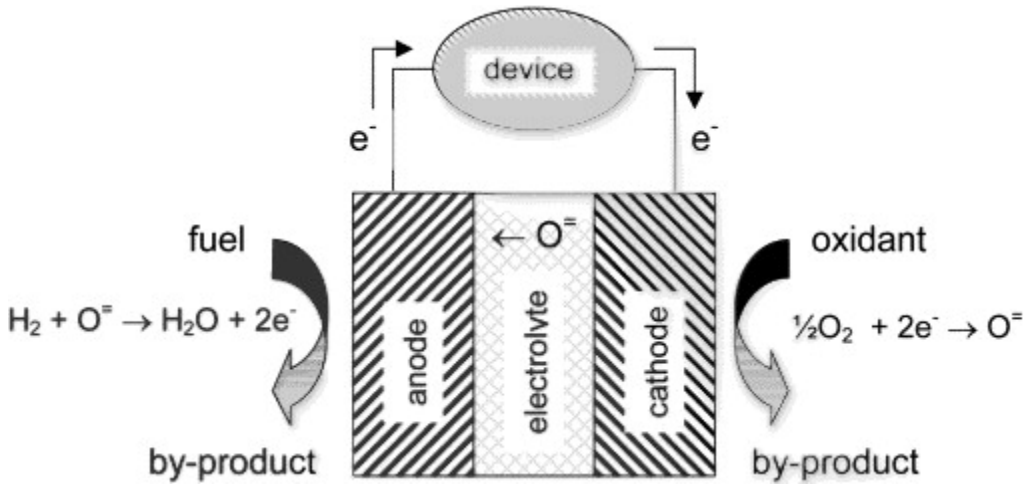

Figure 1: Solid Oxide Fuel Cell Schematic [14]

During the course of the fuel cell's electrochemical process, oxygen atoms from the oxidant travel into the cathode, where they are reduced using electrons provided by the external circuit to create O^{2-} ions. These oxygen ions then pass through the electrolyte to the anode side, where they are met by hydrogen molecules from the fuel source. These hydrogen molecules and oxygen ions react at the anode to create water molecules with 2 leftover electrons. The water exits as a fuel by-product and the electrons travel along the external circuit from the anode to the cathode in order to meet oxygen atoms from the oxidant, allowing for power production to occur. In lower-temperature fuel cells, an electrocatalyst is required to speed up this process to make the system viable [14]. By allowing oxygen ions to pass through the fuel cell towards the fuel source, chemical reactions with the hydrogen atoms can occur, producing power for a necessary electrical load. [14,15]

SOFCs are a specific type of fuel cell in which the electrolyte is a solid ceramic oxide material splitting the porous cathode and anode. This forces these fuel cells to operate

at a far higher temperature (700 – 1000 °C) than standard fuel cells, though reducing the thickness of the electrolyte or using highly conductive electrolytes can reduce the overall temperature requirements [16]. The high temperature requirements drive the costs of SOFC production up significantly, and efforts to lower the required temperature for more practical usage of SOFCs have been a continuing point of research since their creation [15,17]. However, operation at high temperature also allows for a production of high grade waste heat, and if coupled with a CHP system, SOFC systems can reach efficiencies of 85-90% [18].

SOFCs can also take various shapes, with both planar and tubular modules being commonly used. Tubular SOFCs are typically closed at one end and require less sealant material, but often have larger stresses, cost more to produce, and have lower power densities than planar SOFCs [14,16,18,19]. They can be fabricated either cathode-layer or anode-layer first, and are then coated with electrolyte and the opposite electrode layer [19,20]. Both types of SOFCs can be built to be self-supporting. For this, the anode, electrolyte or cathode layer is typically significantly thicker than the other two in order to provide that self-support [16]. It should also be noted that the overall thinner thickness of planar SOFCs versus tubular SOFCs does allow for higher power densities in planar SOFCs. With planar SOFCs, a large cost is required due to sealing requirements of the cell. The oxidant being supplied to the cathode must be kept away from the fuel source being supplied to the anode, which requires a sealant that will not crack, even at high temperatures. Previously, special metal alloys and ceramic materials have been used for

sealing [15], though their high costs have recently pushed glass-ceramic material research [21–23] as these can be significantly more cost effective [24].

SOFCs are typically fueled with a hydrocarbon fuel source. Due to this, the most common SOFC anode material, Ni-YSZ has large carbon deposition issues, as the nickel left in the anode is a strong catalyst for C-H and C-C bonds. This can degrade SOFC performance if the active sites become blocked with carbon, and finding stronger resistance to carbon deposition has been a priority in SOFC research [8,25,26].

Single SOFC cells can typically produce up to a maximum of 1.2 V of electricity at ambient temperatures using air as the oxidant [18]. As such, typical useable SOFCs are found in a stack in series in order to combine the voltage across cells to a useable amount [15]. This does depend heavily on temperature, pressure, fuel fed to the cell, and the load on the cell however. The high temperatures SOFCs are required to run at decrease this theoretical reversible cell electric potential to around 1 V instead of 1.2 V.

Fuel Cell Measurement Methods

1. Open Circuit Voltage

Open Circuit Voltage (OCV) testing is also a basic test used in fuel cell monitoring. The OCV is the potential difference across the cells electrodes when no current bias is applied. In fact, the theoretical maximum voltage per cell is in reference to the OCV [27], and the OCV is typically what is used in reference to the working voltage of a fuel cell in general. By examining the OCV of the cell over time, the degradation of the cell can be monitored. Additionally, after initial reduction, a working fuel cell should have an OCV somewhere close to the theoretical maximum – any OCV significantly lower could equal

any number of issues with the fuel cell, sealant, or reactor set up [26,28,29]. It could also however signify changes in ambient temperature and pressure. At higher temperatures for example, like with SOFCs, a lower overall OCV is to be expected. The opposite goes for pressure – lower pressures reduce the OCV potential of an SOFC system [30].

2. Polarization Curve

In order to test the performance of fuel cells, several standard tests can be utilized. A commonly used data tool in fuel cell performance analysis is the polarization curve. This plot will show the voltage output of the fuel cell versus specific current density loadings on the cell. This can then be compared to other polarization curves from other research to compare a fuel cell's performance. This test is done by slowly increasing the current density on the fuel cell. A typical polarization curve shows three stages of voltage dropping as the current density is increased on the cell. At very low current densities, the voltage will drop due to activation polarization or kinetic losses due to the energy required to begin or activate the chemical reactions required for fuel cell power production. At high power densities the voltage will rapidly drop due to concentration polarization or mass transfer losses due to the mass transfer resistance of the cathode and anode. Between these two extremes, the voltage typically drops linearly due to ohmic losses, or the electron and ion flow resistance in the fuel cell. By examining this polarization curve, the type and magnitude of the fuel cell's losses can be determined [31].

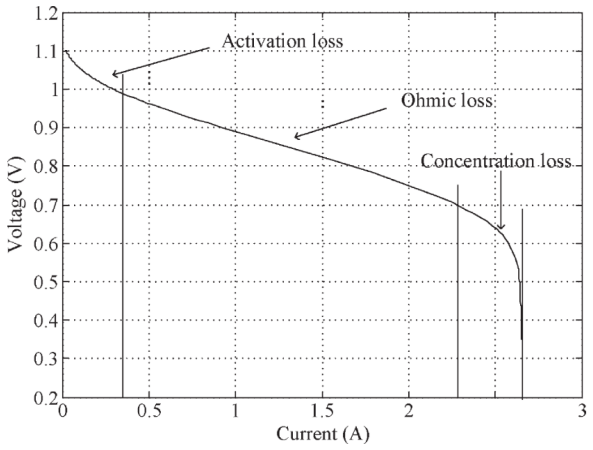

Figure 2: Polarization Curve Example [32]

Mass transfer, or concentration losses occur where there is a limitation on the rate of mass transfer; in fuel cells, this often happens at the anode. This occurs at higher current and power densities, as the flow rate through the anode cannot keep up with the required current rate. This can cause a sharp decrease in cell voltage, as the current is no longer able to be drawn compared to the gas flow rate [33].

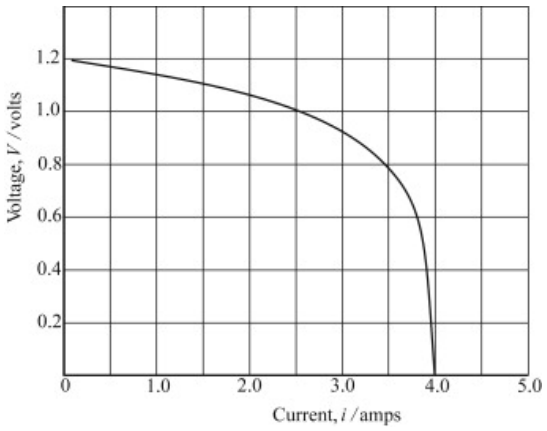

Figure 3: Example of Mass Transfer Losses' Effect on Fuel Cell Voltage [33]

3. Electrochemical Impedance Spectroscopy

Another test that is commonly run in fuel cells is an Electrochemical Impedance Spectroscopy (EIS) test. While EIS testing has been extensively used recently in the biological field to test tissues and cells for various cancers and other diseases [34–36], it can also be used to determine impedance in fuel cells. As frequency is adjusted, EIS determines the overall impedance of the fuel cell. This is typically plotted in a Nyquist or Bode plot. By examining these EIS plots, a fuel cell equivalent circuit can be built using resistors for the real impedance and capacitors and inductors for the imaginary impedance. By showing the equivalent circuit and the inductance and capacitance of different parts of the fuel cell, a better understand of the type of losses in the fuel cell system can be found [37]. The equivalent circuit depend on the types of materials used in the SOFC, and the EIS results obtained during the fuel cell experimentation [38]. An example of an equivalent circuit based on EIS results can be seen in Figure 4.

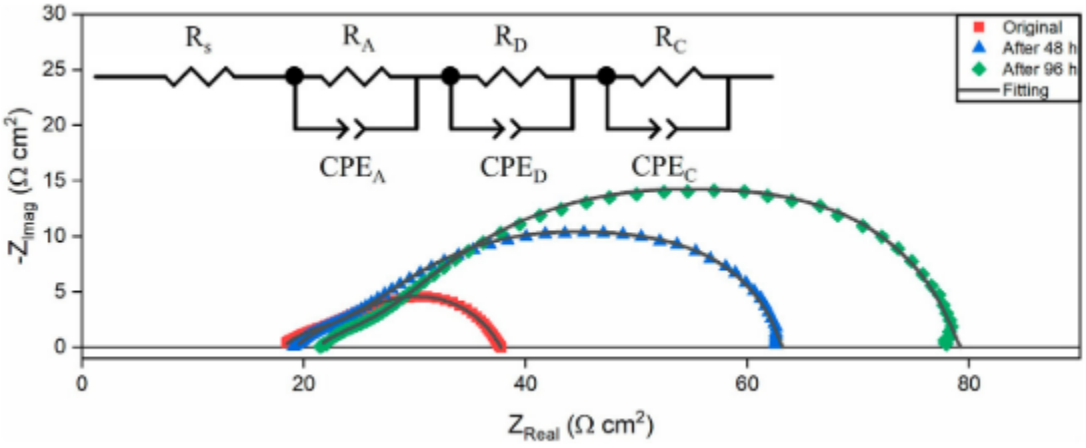

These equivalent circuits allow for a better understanding of the ohmic and polarization resistance, as well as those at the cathode and anode. For example, at high frequencies, the capacitors in the equivalent circuit act as shorts, so the response is solely based on pure resistance, not impedance. This gives the ohmic resistance of the fuel cell (the point where initially, the Nyquist EIS plot crosses the 0 on the y-axis) [39]. The polarization resistance is where the Nyquist plot cross the 0 on the y-axis at the end of the plot, at a low frequency. At low frequencies, the capacitors in the equivalent circuit become 'open' circuits, so the total polarization resistance becomes the sum of the resistances in series, rather than the sum of the resistances with shorts like the ohmic resistance. Additionally, the anode and cathode each can act as one R-C circuit each in the equivalent circuit, allowing for calculation of the capacitance and resistance of each electrode in the fuel cell.

By plotting the EIS data at different stages in a fuel cell's experimentation, the resistance over time can be observed. This is especially apparent in the Bode plots for EIS. It has been suggested, for example, that at low frequencies, any significant changes in the cell's resistance could be due to differences in the diffusion process in the anode [40]. Additionally, at higher frequencies, changes in the cell's resistance could be from changes in the cathode activation polarization [41] and from variations in the internal fuel cell temperatures [42]. This typically implies some change in the oxygen's molecular and charge diffusion ability within the cathode has occurred, and partial pressure of the oxygen is also reduced. Figure 5 below shows the resistance increase of an SOFC over time during a siloxane deposition experiment through a Nyquist EIS plot, showing the degradation of

the cell due to this deposition [43]. These plots allow for better understanding of ohmic and polarization resistance, as well as locating the resistances at the anode and cathode.

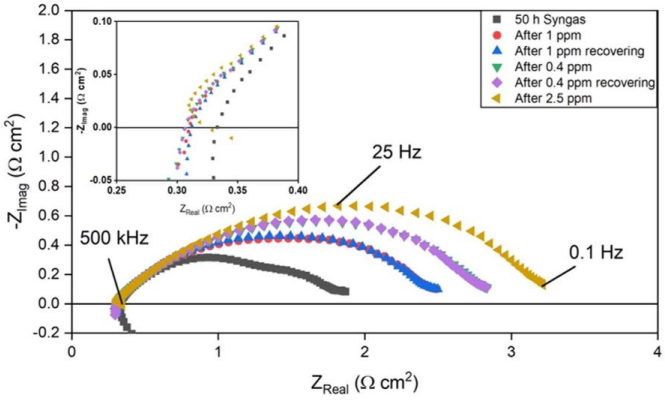

Figure 5: Electrochemical Impedance Spectroscopy Curve Example [43]

4. Gas Chromatography

Gas chromatography is a process in which individual compounds in a gas mixture are separated and analyzed to identify the compounds inside the mixture, typically done inside a gas chromatograph (GC). Inside the GC, the gas mixture passes through a long column, which is coated with a 'stationary phase' material. Typically, the gas mixture is made up of the gas or liquid being tested and a carrier gas which helps guide the mixture through the column. As the gaseous mixture passes through the column, each individual compound adsorbs differently with the stationary phase due to their individual chemical and physical properties, slowing some compounds down more than others and separating them out by the time they reach the end of the column. At this point, the gases are detected and analyzed, and based on the time at each large detection, the gases can be identified by comparing to calibration standards [44,45]. One type of common detector system used (and the type utilized during this thesis) is a Flame Ionization Detector. This detector combusts

the gas, emitting electrons to produce ions, which can then be measured directly as current. This system is especially sensitive to compounds containing carbon atoms, and is relatively low-cost [44,46]. A sample diagram detailing this system can be seen below (Fig. 6).

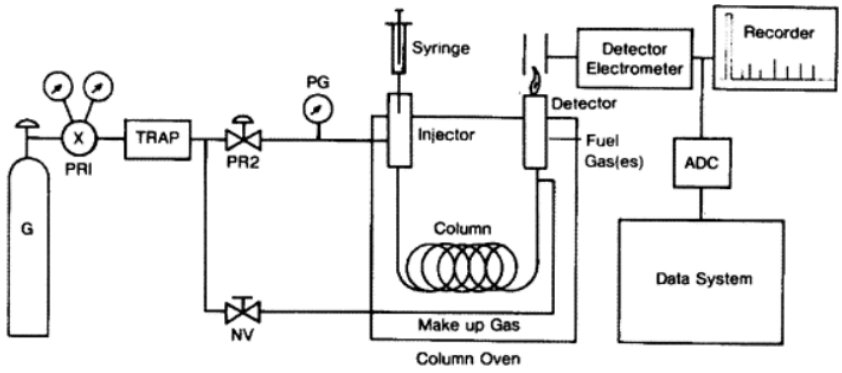

Figure 6: Example Gas Chromatography Schematic [44]

5. Scanning Electron Microscopy

Running an analysis with a scanning electron microscopy (SEM) wallows for understanding the surface topography and chemical structure make up of a given sample. SEM is able to look at samples on a micro-scale, getting resolution down to 1 nm, compared to standard optical microscopes which might only reach 1 μm instead [47]. In an SEM, a focused electron beam is utilized to view the surface of the sample, by reflecting off the various molecules and elements present. As a result of the electrons from the beam hitting the surface of the sample, various signals can be read and analysis completed [48]. These signals vary from backscattered and secondary electrons to x-rays and light [47]. The signals can then be detected and compiled into an image to show specific information about the sample surface. Elemental mapping specifically can be done by energy dispersive

spectroscopy (EDS) or wavelength dispersive spectroscopy (WDS), which uses the x-rays returned from the surface of the sample to map quantities and locations of various elements.

In SOFCs, using SEM has allowed for a better understanding of how contaminants deposit on the anode surface, such as carbon, silicon, and sulfur atoms, which are most commonly found on the anode material. For example, Madi et al. reported a large amount of SiO_2 among the nickel foam used for their anodes [49] and Tian et al. found the silicon bonded near the Ni-YSZ triple-phase boundary interface [43]. Additionally, when using SEM, WDS can be more accurate for SOFCs, as yttria and silicon elements have been noted to have signal overlap, resulting in potentially overestimating the amount of both elements [50].

Siloxanes and Biogas

Siloxanes are man-made chemical compounds that are characterized by having alternating silicon and oxygen atoms bonded to various alkane compounds. Siloxanes are classified based on their structures: either linear (L) or cyclic (D) as seen below in Figure 5, and by their number of silicon atoms present in each molecule. For example, D4 represents a cyclic siloxane with 4 silicon atoms per molecule for example.

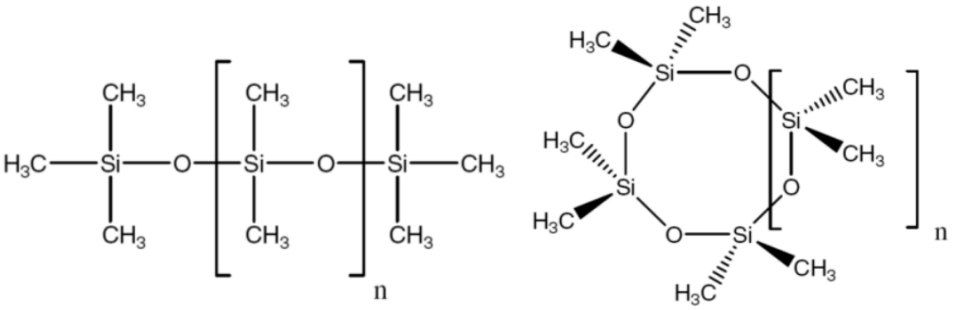

Figure 7: Examples of Linear and Cyclic Siloxanes [51]

Siloxanes also make up silicones, a polymer made up of siloxanes; these are commonly found in a vast array of hygiene products [52], frying oils [53], and contact lenses [54] among others. These siloxanes then end up in wastewater and in landfills – as hygiene products go down sinks, frying oils are dumped into septic tanks, and contacts and other silicon-based products end up in the trash in landfills. Siloxanes are a large contaminant in wastewater treatment processes around the world [55–57] alongside hydrogen sulfide, water, and other small impurities. They have also been found to be a contaminant in both indoor and ambient air [58,59].

Siloxanes have been studied especially in regard to biogas, a potential fuel source created by putting various organic compounds through a process known as anaerobic digestion (AD). AD is typically done in wastewater treatment plants towards the end of the process with sludge that is pulled from clarifiers and is one way WWTPs can dispose of their sludge. Sludge is pumped into an anerobic digester for this process to occur. Inside the digester, microorganisms break down the sludge into this biogas, while in the absence of oxygen. There are two main types of anaerobic digestion. Mesophilic digestion occurs around 30-38℃ while thermophilic digestion requires some additional heat and runs around 50-60℃ [4]. Biogas is also generated from the organic decomposition of solids in landfills [60]. Biogas from wastewater treatment plants is roughly 55-65% methane (CH_4) and 35-45% carbon dioxide (CO_2), which has similar constituents to another fuel source: natural gas. However, biogas also contains trace amounts of several contaminants including ammonia, oxygen, hydrogen sulfide and siloxanes [1]. The contaminants found in the biogas severely limits its potential use as a fuel source, as the siloxanes and other impurities

can deposit on the boilers, CHP prime movers, heat exchangers, and any other equipment that might utilize biogas, which will decrease performance and lifespan of the equipment [4,61]. It has been found specifically that silicon deposits typically form first in reciprocating engines, allowing for increased deposition of the other impurities like calcium and sulfur [62].

There are also several different siloxanes that can be present in biogas, depending on the source of the gas. D4 (octamethylcyclotetrasiloxane) and D5 (decamethylcyclopentasiloxane) siloxanes are typically the most commonly found as contaminants in wastewater and landfills [4,13], though other siloxanes, particularly linear siloxanes have been found to be more abundantly used in products that might end up in landfills and wastewater [63]. D4, D5, and other cyclic siloxanes have been suggested to be the most prevalent siloxane contaminants due to their structural stability, which may explain their prevalence in landfill and wastewater biogas compared to linear siloxanes [13]. Because of D4 and D5's prevalence in both landfill and wastewater biogas, experiments run to determine siloxane degradation's effects on SOFCs and other power-producing prime movers, typically focus on these two siloxanes [11,43,64,65]. Table 1 below gives some approximate values for various siloxanes found in both landfill and wastewater biogas. While the values themselves vary largely from study to study, some interesting trends develop. For example, in both landfill and wastewater-produced biogas, D4 and D5 siloxanes have the largest concentrations, and often by magnitudes of 5 or more. Additionally, D3 (and D6 siloxane where studied) also had larger concentrations than both L3 and L4 siloxanes for both landfill and wastewater-produced biogases. In biogas from

WWTPs, L2 was also lower than D3, though this did not always hold true for biogas from landfills.

Table 1: Siloxane Concentrations in Landfill and Wastewater Biogas (in mg/m^3)

Biogas Source	L2	L3	L4	D3	D4	D5	D6	Source
Landfill	n.d.	n.d.	n.d.	5.9 ± 0.3	49.1 ± 0.2	16.6 ± 0.1	n.d.	[12]
	0.837 ± 0.151	0.614 ± 0.089	0.506 ± 0.104	0.874 ± 0.180	4.159 ± 0.627	2.896 ± 0.448	0.659 ± 0.153	[13]
	0.565 ± 0.154	0.023 ± 0.007	0.006 ± 0.004	0.129 ± 0.083	1.083 ± 0.276	1.135 ± 0.293	n.d.	[66]
Waste water	n.d.	n.d.	n.d.	0.7 ± 0.2	2.6 ± 0.2	11.6 ± 0.3	n.d.	[12]
	<0.01	0.28	0.31	0.12	1.9	124	n.d.	[67]
	0.05	0.03	0.13-0.15	0.14-0.17	6.40-6.98	8.96-9.65	n.d.	[68]

Siloxane use with SOFCs

When biogas is utilized in SOFC systems without cleaning, the siloxanes will deposit on the surface of the anode which will reduce the cell's performance. As the fuel source's hydrogen atoms meet oxygen ions in the anode, water molecules and electrons are created as follows:

$$H_2 + O^{2-} \rightarrow H_2O + 2e^-$$

However, with additional impurities like siloxanes and sulfides, these output molecules may react to create silicon oxide on the anode surface. Haga et al. in 2008 proposed the following chemical reaction equations to show how D5 siloxane would deposit silicon dioxide molecules into the anode [5]:

$$Step\ 1\text{: } [(CH_3)_2SiO]_5(g) + 25\ H_2O \rightarrow 5\ Si(OH)_4(g) + 10\ CO + 30\ H_2$$

$$Step\ 2\text{: } Si(OH)_4(g) \rightarrow SiO_2(s) + 2\ H_2O$$

From these proposed equations, it was assumed that silicon dioxide would deposit on the anode surface, which can decrease overall gas diffusion through the anode and increase overall polarization resistance of the SOFC [69]. Additionally, silicon-carbon bonds from the siloxanes can break off and deposit on the anode, depositing silicon not only as SiO_2 but also as SiC [43]. It has also been suggested that CH_4 can be deposited on the anode due to siloxane degradation [43].

3. FUEL CELL FABRICATION

Ni-SDC SOFC Fabrication

Anode-supported SOFCs were fabricated using a process from previously reported work [50].

1. Anode Fabrication

The anode was fabricated first using a mix of nickel oxide (NiO, Fuelcellmaterials) and samarium-doped ceria (SDC, $Sm_{0.20}Ce_{0.80}O_{2-X}$, Fuelcellmaterials). The NiO and SDC powders were mixed using a mortar and pestle at a 60:40 weight ratio, respectively, until a homogenous mixture was created.

Figure 8: Mortar and Pestle Used for Nio+SDC Powder Mixing

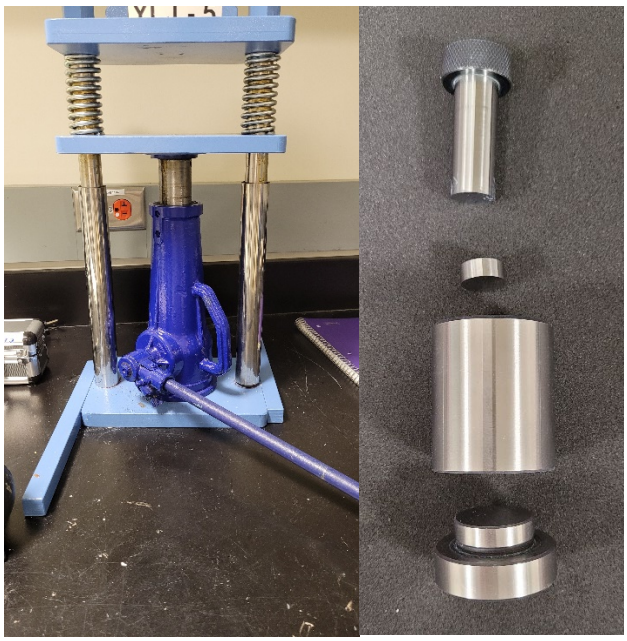

Figure 9: Dry Press and Dry Pressing Die Used to Create Ceramic Anode Discs

After pre-sintering, an SDC electrolyte was prepared for use in a wet powder spray machine by using a mixture of SDC, ethyl alcohol, ethylene glycol, and glycerol and running that mixture in a ball mill for roughly 24 hours. Once the wet spray was mixed, a spraying machine (Sono-Tek) was utilized to spray even layers of the SDC wet powder spray onto the NiO+SDC ceramic discs. These discs were placed on a heating plate as seen below in Figure 8 and heated to roughly 90℃ through the spraying process. One layer of spray was administered to the cells, then the heating plate temperature was increased to roughly 160℃ before being decreased back to 90℃. This process between each individual spray layer allowed for the evaporation of ethyl alcohol and ethylene glycol from the sprayed layers. 17 layers of SDC wet spray material was sprayed onto the NiO+SDC ceramic discs. The anode-electrolyte discs were then pre-sintered at 1350℃ for 4 hours.

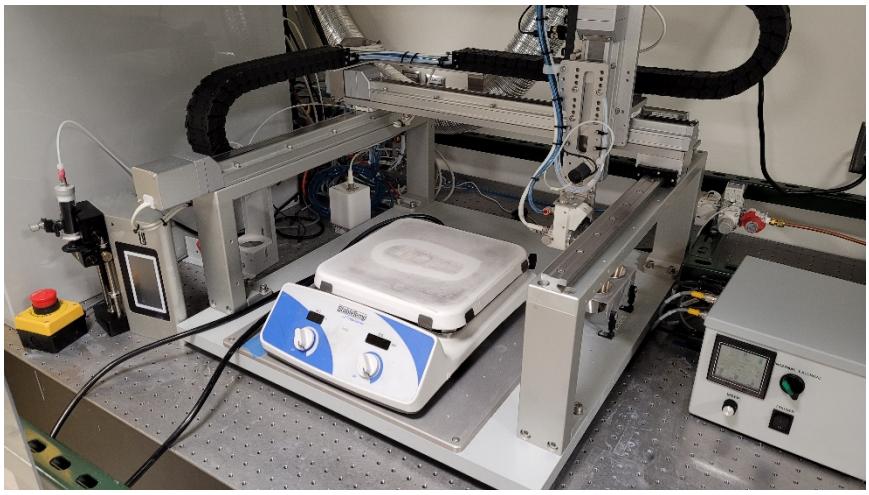

Figure 10: Sono-Tek Spraying Machine and Hot Plate Used for Wet Powder Spray

A yttria-stabilized zirconia (YSZ, $(ZrO_2)_{0.92}(Y_2O_3)_{0.08}$, Fuelcellmaterials) buffer layer wet powder spray mixture was then created using ethyl alcohol, ethylene glycol, and glycerol and left in a ball milling machine for 24 hours. This mixture was then sprayed onto the anode-electrolyte discs using the same process as before for 6 layers. The anode-electrolyte-buffer layer disc was then co-sintered at 1400°C for 4 hours.

4. Cathode Fabrication

Finally, a lanthanum strontium manganite (LSM, $(La_{0.80}Sr_{0.20})_{0.95}MnO_{3-X}$) + YSZ (Fuelcellmaterials) cathode wet powder spray was also then produced using the same process as before. This was sprayed onto the ceramic discs using a hand sprayer as seen below.

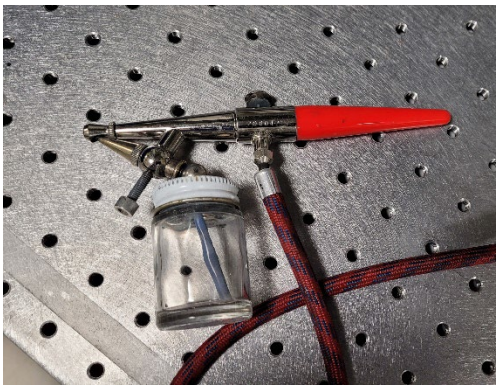

Figure 11: Hand Spray Machine Used for Cathode Wet Powder Spraying

6. Fabrication Failures

These SDC-supported fuel cells were to be used for experimentation, however due to electrical and physical failures, other, YSZ-supported fuel cells were utilized for experimentation. The first attempt at creating SDC-supported fuel cells used the dry press for the anode and electrolyte layers, instead of just the anode. For this first batch, the anode was dry pressed exactly as described previously, but then 0.04 g of SDC ceramic powder was dry pressed on top of the un-sintered anode layer. This anode-electrolyte pressed disc was then pre-sintered at 1100°C for 2 hours. Due to differences in material porosity, density, and the thickness of the electrolyte layer, these cells all curled inwards and most cracked, preventing testing. Some of these cells can be seen below.

Figure 12: Double-Pressed SOFC Fabrication Attempt Results

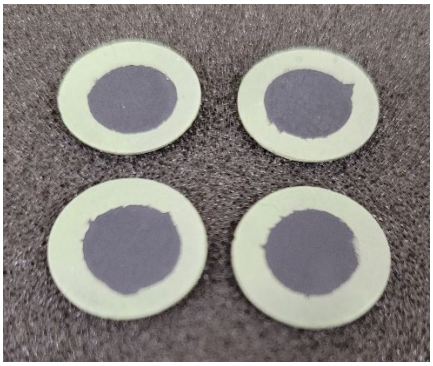

Figure 13: Fabricated SDC-Supported Fuel Cells

materials may have been less smooth and had higher potential for large peaks and valleys. This could potentially allow for easier transport of electrons throughout both the anode and electrolyte layers. When the buffer layer was sprayed onto the surface of the electrolyte as a full-stop for the electrons, some of these porous valleys may not have been filled fully in, allowing for electrons to pass through the fuel cell directly from the anode to the cathode side, rather than being stopped by the buffer layer. This may be one cause of the reduced performance. SOFCs were produced with 12 layers of buffer layer spray instead of the 6 layers originally used which did produce a higher OCV; however these results were still significantly lower than the 1 volt SOFC maximum at 800°C and were also ruled not significantly testable (maximum OCV of 0.63).

These failures could also simply be the result of human inaccuracy – any slight imperfection could be a cause of the decreased performance. The sizing of each individual planar layer was also estimated based on previous work with YSZ-supported cells [43,50] and will need additional research to confirm the optimum size of each portion of the cell. Additionally, while Ni-YSZ anodes for SOFCs have been thoroughly researched, Ni-SDC anodes have been researched significantly less over the last 30 years [25,26,70,71], and will need further research to solidify a dry-pressing and wet powder spraying method to make them feasible for experimentation.

Thus, after testing these SDC-supported cells post-reduction with EIS tests, OCV tests, and polarization curves, they were found to be inadequate for our experiments. Several sets of these SDC-supported fuel cells were produced, each of which had similar

poor electrical results. As such, YSZ-supported SOFCs were instead used for experimentation. These were produced a similar process to that presented above [50].

Ni-YSZ SOFC Fabrication

A 60/40 weight ratio mixture of NiO and YSZ was first mixed in a mortar and pestle to create the Ni-YSZ homogenous mixture that would be used for the anodes. This powder mixture was then dry pressed with 0.3 g of material, and was then pre-sintered at 1100°C for 4 hours to allow for densification of the powder particles. This created a ~ 380 μm thick anode layer for the anode supported SOFC. These ceramic discs were also 0.712 cm^2 in surface area.

Once the anode had been sintered, a YSZ electrolyte mixture was sprayed onto the anodes using the same Sono-Tek spraying machine set up as before, using a similar mixture of YSZ powder, ethyl alcohol, ethylene glycol, and glycerol as the spray mixture. Between each layer of spray, the heating plate was again heated to roughly 160°C before being allowed to cool to 90°C for evaporation of ethyl alcohol and ethylene glycol. Once the electrolyte had been sprayed onto the cells, they were once again pre-sintered to allow for densification of the electrolyte. The electrolyte ended up around ~ 10 μm thick.

A ~ 3 μm buffer layer of SDC was then sprayed onto the electrolyte, using a spray mixture of SDC powder, ethyl alcohol, ethylene glycol, and glycerol. This was also done with the Sono-Tek spray machine, and again the heating plate was heated to 160°C and allowed to cool to 90°C between sprays. The anode-electrolyte-buffer layer discs were then co-sintered at 1400°C for 4 hours. After this, the hand spray machine was used with a

mixture of lanthanum strontium cobalt ferrite (LSCF, $(La_{0.6}Sr_{0.4})_{0.95}Co_{0.2}Fe_{0.8}O_{3-X}$, Fuelcellmaterials) + SDC (70/30 weight ratio), ethyl alcohol, ethylene glycol, and glycerol to create the cathode layer. Again, the edges were taped off of each cell to prevent the cathode from slipping down the side of the SOFC and creating a short with the anode. The discs were sprayed on the heating plate and between each layer of spray, the plate was heated to 160℃ and allowed to cool to 90℃. The SOFCs were then sintered to 1100℃ for 2 hours, creating a ~ 17 μm thick cathode and finishing the fabrication of the Ni-YSZ SOFCs used in this experiment.

4. EXPERIMENTAL SET UP

For this investigation, degradation in a YSZ-supported SOFC using L4 siloxane ($C_{10}H_{30}O_3Si_4$) is being tested. As such, for the experiment, L4 siloxane along with H_2 and N_2 gases were used as the fuel source. An experimental set up as shown below in Figure 14 was established.

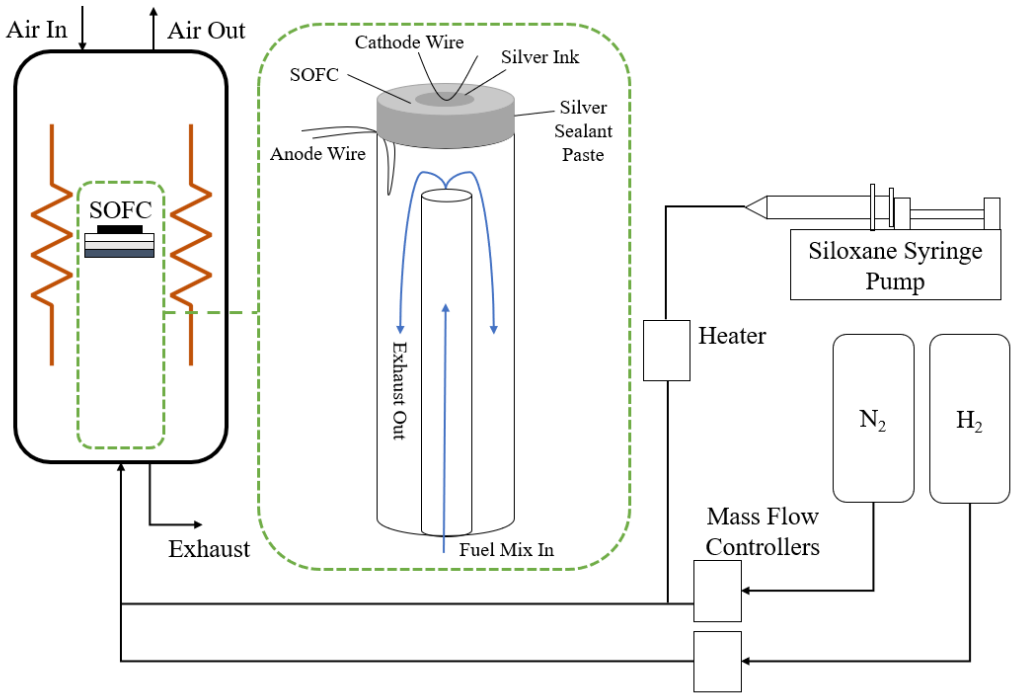

Figure 14: Experimental Setup

The fuel cell was sealed to a quartz tube using silver paste, which served both to prevent any leakage of the fuel source and to act as the current collector connecting the anode to the cathode. The quartz tube reactor was then placed inside the sealed quartz tube, which allowed for the fuel to flow towards the fuel cell through the reactor and back out as exhaust through the sealed quartz tubing. The exhaust was left open inside a fume hood

and was used later for GC testing using sealed bags to collect it. Siloxane was directly pumped through piping into the reactor via a syringe pump system (Pump Systems Inc. Ne-300 Just Infusion), while both N_2 and H_2 gases were pushed through piping and Brooks Delta II smart mass flow controllers (MFCs). Air was used as the oxidant for these experiments. The fuel cell and quartz tubing was placed inside a furnace (MTI Corp GSL1100X) and heated slowly up to 800℃, at a rate of roughly 5℃ per minute. All experiments were run continuously with a furnace temperature of 800℃. The gas flow rates were held constant by the MFCs and syringe pump system for each experiment at 20 milliliters per minute (mL/min) of H_2, 10 mL/min of N_2 and 0.15 mL/min of Siloxane for 0.5% impurity in the fuel source.

The cells' performances were measured using the 4-probe technique with the I-V (current-voltage) method. Silver and steel wiring was used. The probes were connected to an Electrochemical Impedance Analyzer (Solartron Analytical Energylab XM), which was connected to a computer for testing the EIS of the fuel cells.

The experiments were run as follows:

1. H_2 and N_2 was supplied as the fuel source with no siloxanes for roughly 2 hours after the furnace reached 800℃, allowing for reduction of the anode. The siloxane pump was still connected to the system to avoid the H_2 and N_2 gases from escaping before the reactor, but was powered off.
2. Once reduction was complete, the siloxane pump was initiated, allowing for siloxane degradation of the SOFC to begin. Every 30 minutes, an EIS test and

polarization curve were completed, and a sealed bag of exhaust was collected for use in the GC. OCV was monitored continuously for each 30 minute interval.

3. After the first 4 hours of siloxane poisoning, not including the reduction time, a continuous current density of 100 mA/cm^2 was applied and a continuous data-reading of the voltage until the cell's failure was recorded.

5. RESULTS

Several papers have previously researched the effects of D4 siloxane contamination on Ni-YSZ based SOFCs [43,49,50], but as far as can be found, only one has been done on L4 siloxane [11]. As such, the focus of these experiments was to determine the effects of L4 siloxane on the SOFC degradation. To accomplish this, several tests were completed to test the power density and voltage over time as well as the composition of the exhaust gases. These results were only gathered once the anodes had been reduced for 2 hours, though this may not have been enough time to fully reduce the cells. An Electrochemical Impedance Analyzer (Solartron Analytical Energylab XM) with its XM-Studio Software was utilized to gather data on fuel cell impedance, voltage, and power density. Uncertainty is rated for this equipment at 0.1% for polarization and 0.01% for frequency [72]. As such, no error bars or uncertainty analysis will be presented on the plots for the results.

OCV and Constant Current Curves

This is potentially evident in the OCV curve seen in Figure 13, as the OCV increases for roughly 80 minutes after the tests began before stabilizing then starting to decrease due to the siloxane deposition. Typically, as the anode reduces, the OCV will increase until full anode reduction, when siloxane deposition begins to occur and degrade the SOFC's performance. This can be seen around the 100 minute mark, as the cell's performance levels out before beginning to degrade. It should also be noted that the OCV recorded during the first 240 minutes of experimentation still remains relatively stable, even though a slight degradation is observed after 100 minutes. The range for the OCV over the first 240 minutes is only from 0.975 V to 1 V, a 2.5% difference.

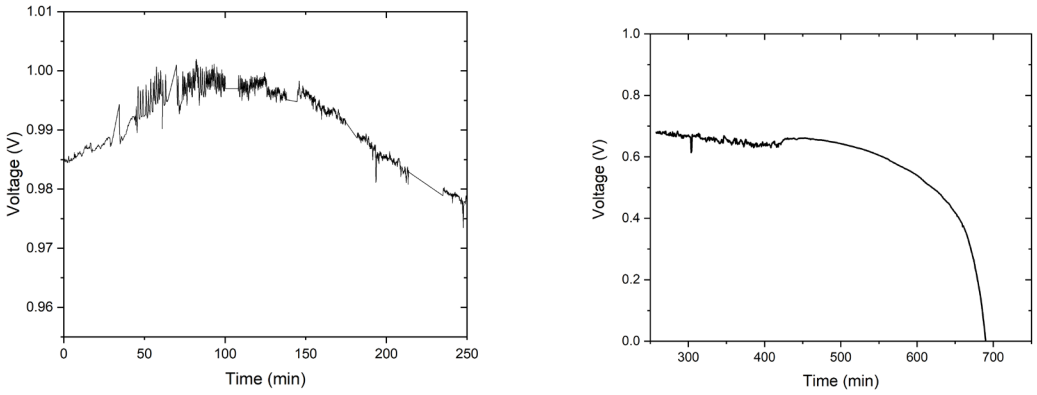

Figure 15: OCV Curve and Constant Current Curve Showing Voltage Drop Over Time

After the initial tests were run for roughly 240 minutes, a constant current test was run until the cell's failure. The cell initially continued to decline at a steady rate until approximately 7 hours (420 minutes) into the experiment, when it began to steady out and then decline at an exponential rate until voltage reached 0 around 690 minutes (11.5 hours) into the experiment. These results indicate that siloxane deposition has a significant effect on the SOFC's performance as other literature suggests that without siloxanes, or even with lower concentrations of siloxanes present, similar Ni-YSZ SOFCs can run for hundreds of hours [7,43,50].

SOFC Coloration and Physical Results

Another SOFC was also run only to the full anode reduction stage in order to determine if any physical differences could be noted between the anode post-siloxane deposition and pre-siloxane deposition. Typically, it is expected that siloxane deposition results in a yellow/brown color being present on the anode [43], however as seen below in Figure 16, this was not present for this SOFC.

Figure 16: (1) SOFC Anode After Reduction, Before Siloxane Added to Fuel Source and (2) After L4 Siloxane Experiment

The SOFC on the left shows the SOFC post-siloxane deposition, but does not show the typical yellow/brown deposition associated with siloxanes. Instead, it shows as green with gray splotches around the edges, close to the silver paste sealant. Whereas, the SOFC that underwent only reduction shows as completely grey due to the reduction of the NiO inside the Ni-YSZ anode. This is especially intriguing, as the green coloration of the SOFC suggests the cell was not reduced. There are a few possibilities that may explain this coloration.

The first possibility is simply that the silver sealant required to stop the flow of oxygen to the anode was not fully sealed. This would result in oxygen flowing to both the cathode and the anode, and no cell reduction would occur. However, it is clear that some reduction occurred at the anode, due to the gray splotches around the edges. Another possibility theorized was that the silicon or carbon created a thin, clear layer across the entire anode. This in turn trapped the oxygen ions flowing across the electrolyte in the anode, rather than allowing it to fully escape in water molecules, re-oxidizing the anode. Noting from the OCV and constant current curves that there was swift cell deterioration of

performance, the second option seemed more plausible than the first. In order to determine the actual effects, several further tests were completed.

Polarization Curves

The polarization curves for the cell under siloxane deposition can be seen below. These curves suggest a degradation in overall fuel cell performance as the voltage and power density both decreased with elongated exposure to L4 siloxane. The degradation rate for the SOFC after 30 minutes with 0.5% siloxane contamination shows roughly an 8%/30 min decrease in power density as the maximum power density drops from 238 mW/cm^2 to 218 mW/cm^2. Additionally, after 4 hours of siloxane deposition, the cell's maximum power density had dropped 38.7% from 238 mW/cm^2 to 146 mW/cm^2, suggesting additional cell degradation. It should be noted that the degradation slowed significantly after two hours of experimentation, though the siloxane feed rate was not modified during the experiment. Due to this decreased degradation, after 120 minutes, the next data point was gathered at 240 minutes, or 120 minutes after the previous data point. This matches similar findings in other research, noting that the initial degradation was much larger, then was stabilized over time [50,73]. However, the rapid drop-off of voltage as seen above in Figure 15 has not been presented in similar literature. This is most likely due to mass transfer losses in the cell, as after running for extended amounts of time, deposition of silicon and carbon may have prevented the gas flow rate from penetrating the anode enough to keep up with the required high constant current density. It should be noted that polarization curves were not able to be collected after the cell's failure and thus are not presented in Figure 17.

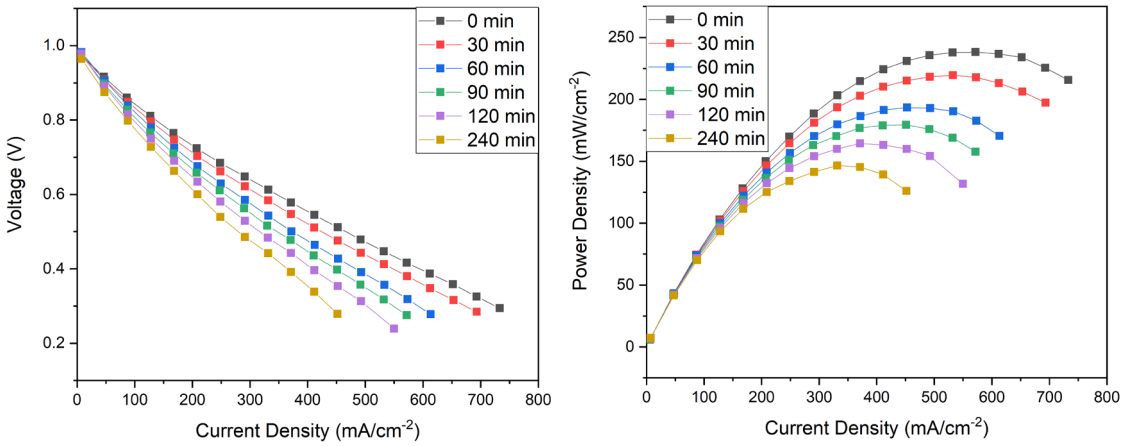

Figure 17: Polarization Curves for Siloxane Degradation

EIS Test Results and Voltage Degradation Rates

EIS test results were also recorded at each of these intervals in order to determine the SOFC's area specific resistance (ASR) increase rate, which is calculated by subtracting the initial cell resistance from the final resistance found in the EIS test. The ASR results for each time interval are seen below in Table 2 based on the results shown in Figure 18 below. Additionally, the voltage rate change per hour was also determined based on the previous OCV curve results. As seen in Table 2, the voltage continued increasing until around 90 minutes when it started decreasing. Additionally, the ASR increases rapidly through the first 60 minutes of the experiment, before beginning to increase more and more slowly as the experiment went on. By 240 minutes, the resistance was hardly increasing. This makes sense – as the initial deposition begins, a larger amount of surface area is present for deposition, allowing for a rapid increase in cell resistance. However, as more and more silicon and carbon are deposited on the cell surface, there is less area for flow rate-blocking deposition to occur, slowing that increase in resistance overall. It still increases, as there is additional deposition occurring, but not as significantly. Once the cell fails, resistance

spikes as very little voltage is able to be carried by the cell. As some current is running, this means a required higher resistance must occur due to the high current and low to nonexistent voltage.

EIS tests confirmed this deposition's effect on degradation. As seen below in Figure 18, at low frequencies, the resistance increases over time during the experiment. Once the cell has failed, resistance increases across all frequencies as well. As previously mentioned, changes in the SOFC's resistance at low frequencies has been suggested to represent changes in the diffusion process in the anode [40], which would suggest deposition of some material on the anode was reducing the total mass transport available to the SOFC.

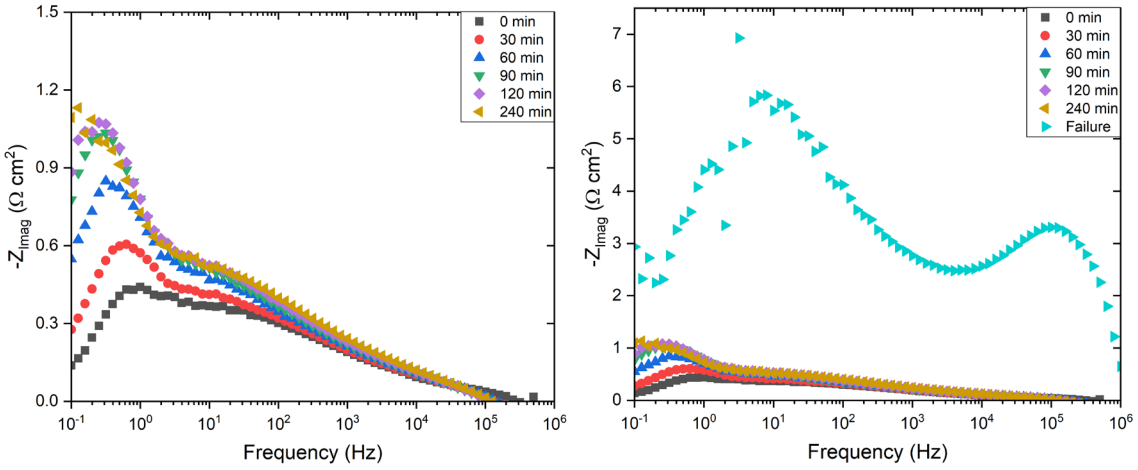

Figure 18: EIS Bode Plots for Siloxane Degradation

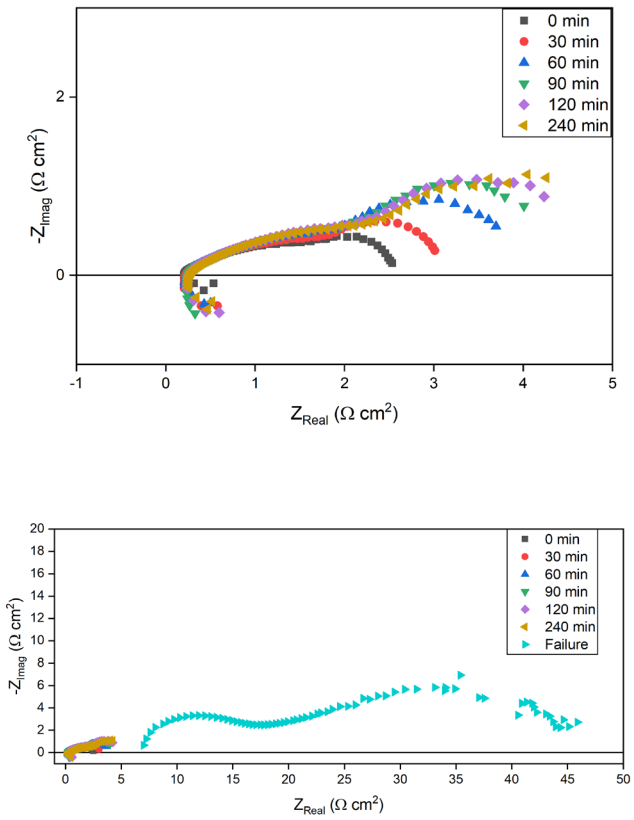

Figure 19: EIS Nyquist Plots for Siloxane Degradation

Table 2: Voltage Degradation Rate and Area Specific Resistance Increase Rates

Time	0 min	30 min	60 min	90 min	120 min	240 min	Failure
Voltage Decreasing Rate (mV h^{-1})	--	--	--	--	-3.82	-8.35	-130.45
ASR (Ωcm^2)	2.324	2.788	3.460	3.755	3.973	3.987	37.612
% Increase ASR / Hour	--	39.9%	48.2%	17.1%	11.6%	0.2%	129.7%

Similarly to the OCV results shown above, the degradation rate from the EIS test shows slowly increasing degradation, before a period of slowing degradation, followed by a rapid degradation until SOFC failure. Again the degradation from 120 minutes to 240 minutes was very minimal, but a large drop-off occurred between 240 minutes and failure at 690 minutes.

The voltage degradation rates can be compared to those given by running a similar Ni-YSZ anode SOFC without siloxane in the fuel source. As seen below in Figure 20 from data gathered by Jiashen Tian, over a 50 hour time period, there was significantly less degradation in the SOFC without siloxanes being present in the fuel source. Degradation here was roughly 0.26 mV per hour over the course of 50 hours, versus the 3.82 and 8.35 mV/hr rates found in this experiment with siloxanes in the fuel source.

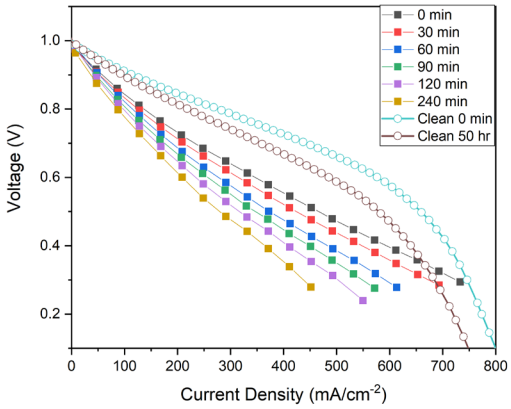

Figure 20: Polarization Curve for Ni-YSZ Anode SOFC without Siloxanes in Fuel

SEM / WDS Elemental Mapping

SEM results using WDS were also gathered at the electrolyte-anode interface, through a cross-section of the anode and at the bottom of the anode, where the fuel source interacted with it. As seen below in Figure 21, at the bottom of the anode, a layer of silicon is very clearly present. The silicon layer appears to have deposited on the surface of the anode, and the carbon layer seen is due to an epoxy used for SEM purposes, and is not indicative of carbon deposition. This would block hydrogen ions from being transported into the triple-phase boundary at the electrolyte-anode interface. This would also imply that with no hydrogens ions to bond with, the oxygen ions became locked in the anode, which could confirm the previously theorized reason for anode re-oxidization. Oxygen ions would still be flowing through the electrolyte, as current was still being applied throughout the SOFC.

It is interesting to note that the oxygen mapped by WDS has the hightest intentsity in the nickel compared to yttria or zirconia, potentially showing that the oxygen did re-oxidize the anode by bonding again with the nickel, creating NiO. This specifically can also be noted in Figures 22 and 23, at the electrolyte-anode interface and throughout the anode cross section suggesting this occurred throughout the entire anode, and not just at the surface. Oxygen is also heavily seen at the bottom of the anode, just above the silicon layer. This could suggest that the silicon and oxygen bonded to form SiO_2, which has been documented previously for SOFCs under siloxane contamination [5,50].

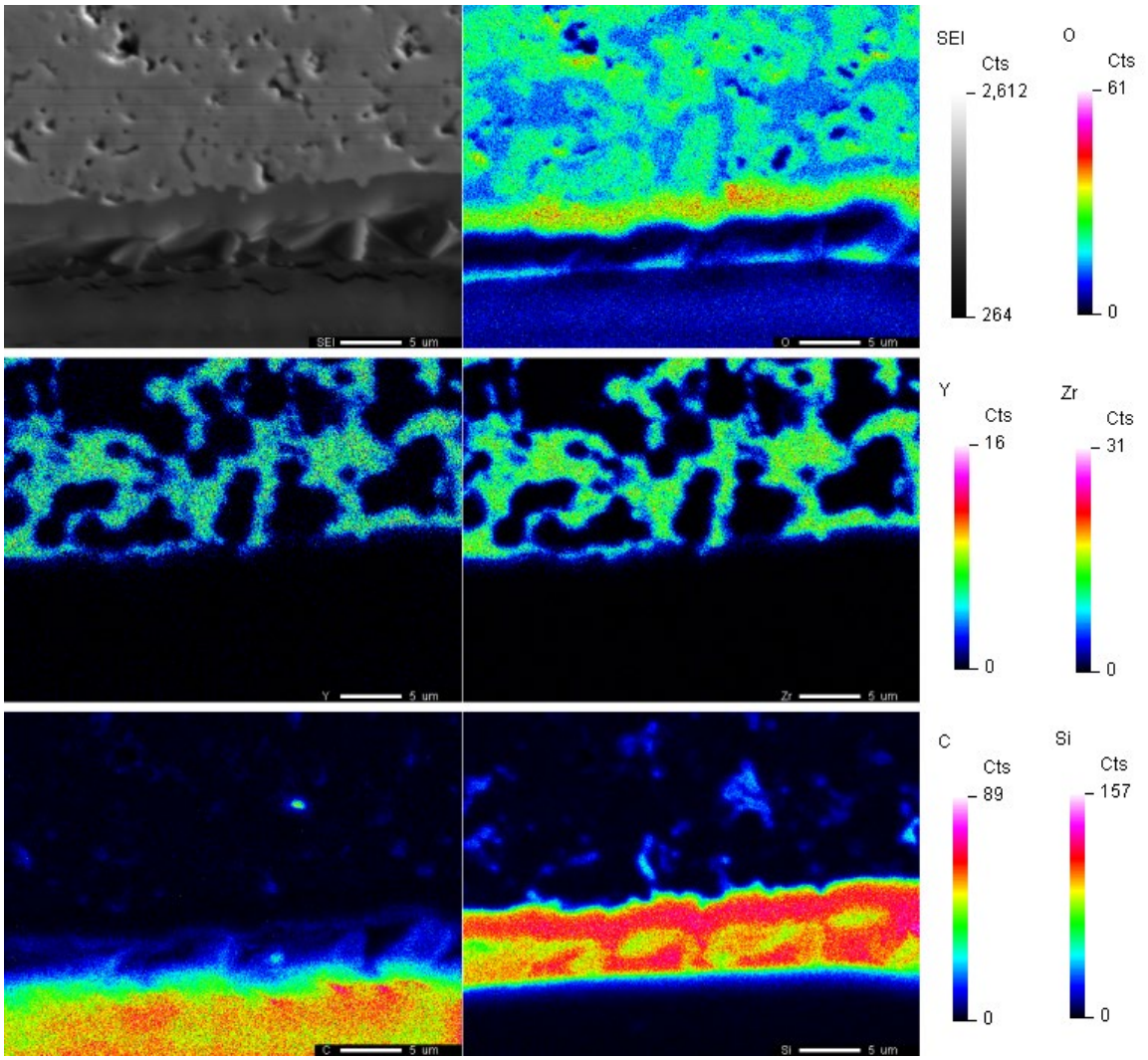

Figure 21: WDS Elemental Mapping of the Bottom of the Ni-YSZ Anode with L4 Siloxane Contamination after SOFC Failure

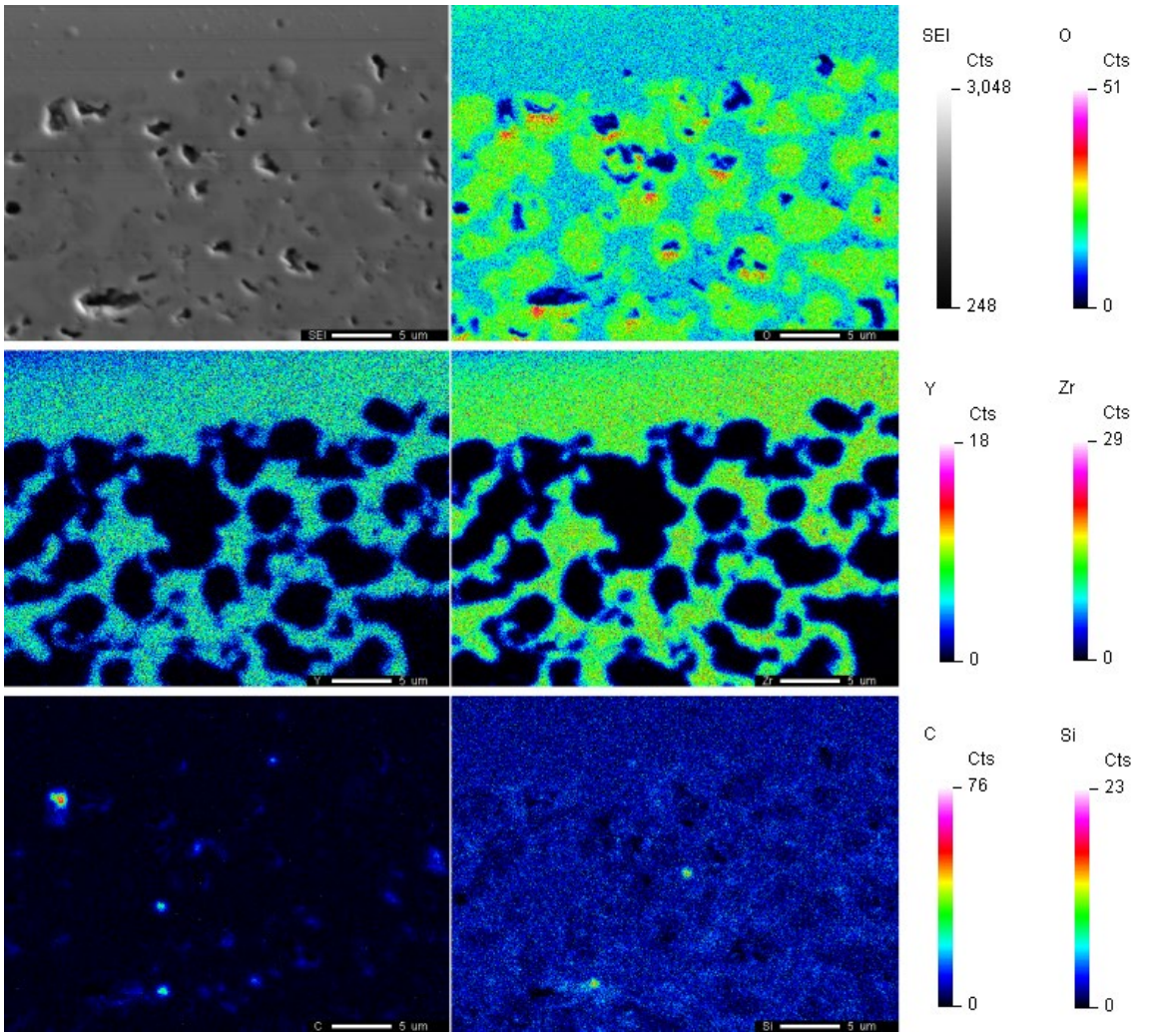

Figure 22: WDS Elemental Mapping of the Electrolyte-Anode Interface with L4 Siloxane Contamination after SOFC Failure

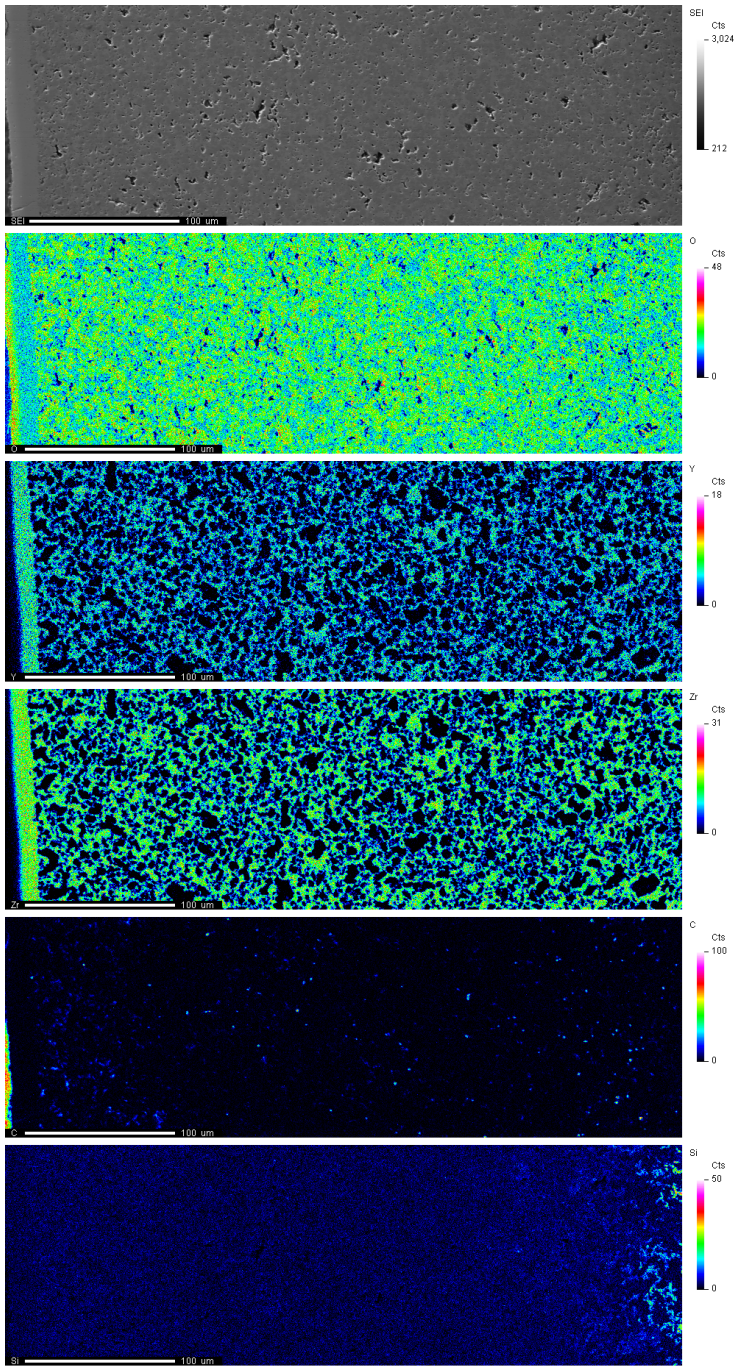

Figure 23: WDS Elemental Mapping Across the Anode Cross-Section with L4 Siloxane Contamination after SOFC Failure (Left Side Showing the Electrolyte, Right Side Showing the Bottom of the Anode)

Gas Chromatography

Additionally, GC results were obtained at 30 minute intervals during the experiment to determine the composition of exhaust gases. This allows for a better understanding of the chemical processes happening in the anode and at the fuel source. Input gases were H_2 at 20 mL/min, N_2 at 10 mL/min and L4 siloxane ($C_{10}H_{30}O_3Si_4$) at 0.15 mL/min. As such, the input air would be expected to be roughly 66.3% hydrogen, 33.2% nitrogen, and 0.5% siloxane. The GC results can be seen in Figure 24.

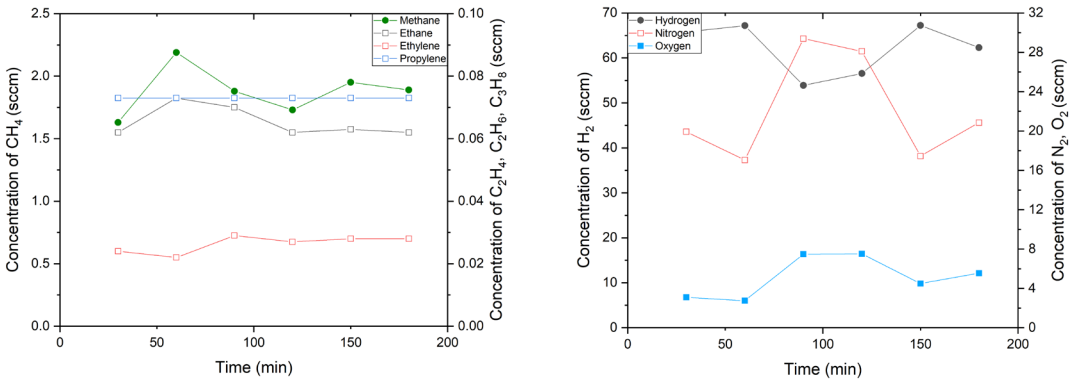

Figure 24: Gas Chromatography Results

As seen in Figure 24, during the experiment, hydrocarbon exhaust tended to follow a similar trend across methane (CH_4), ethane (C_2H_6), and ethylene (C_2H_4), though propylene (C_3H_6) concentration stayed the same throughout the experiment. This release of methane especially could be due to L4 siloxane reacting with the H_2O coming from the fuel cell's reaction to create D3 which was also noted at the 30 and 60 minute mark in a separate GC investigation. That reaction has been proposed before as [74]:

$$D3 + TMSOH\ Creation\text{: } C_{10}H_{30}O_3Si_4 + H_2O \rightarrow C_6H_{18}O_3Si_3 + (CH_3)_3SiOH + CH_4$$

This reaction may give some indiciation of the increase in methane production during the first 60 minutes of the experiment. As seen in Figure 19, CH_4, C_2H_6, and C_2H_4 all follow an increase-decrease pattern over the course of the experiment. Additionally, the 2nd rise and fall around 150 minutes is significantly smaller than the initial bump around 60-90 minutes.

Additionally, hydrogen in the exhaust was signfcantly lower from 90-120 minutes than before and after, while nitrogen and oxygen increased during that interval. This indicates that during this time, hydrogen gas was removed from the fuel source at large rates. This could be due to the unfinished reduction noted earlier. The large decrease in hydrogen is particularly noticeable around this time. It may be that once the reduction was closer to being finalized, oxygen ions were able to connect with hydrogen atoms at a higher rate, rapidly converting large amounts of hydrogen and oxygen ions into water. Water buildup was noted in the exhaust pipe at several points during the experiment, and was vaccuumed out during those points. Additionally, carbon monoxide from the siloxanes and hydrogen gas may have been reacting to form additional water and individual carbon atoms, which may have deposited on the anode instead. This could also decrease the overall hydrogen exhaust. Interestingly, during those times, nitrogen and oxygen were more prevalent in the exhaust gases – though if this is due to a lower amount of hydrogen being present, this could simply be due to the overall output of gas being signifcantly lower than before.

6. CONCLUSION

L4 siloxane is one impurity found in biogas produced in landfills and WWTPs that can harm the lifespan and feasibility of prime movers, if biogas is utilized as a fuel source. As such, an experiment was completed to determine what effects L4 siloxane would have on a Ni-YSZ based SOFC. These tests utilized siloxane, N_2, and H_2 as a fuel source, and tested the siloxane deposition's effect on the SOFC's voltage and power density degradation, as well as overall resistance increase. These tests were calculated using EIS, OCV, and polarization curves. GC data was also gathered to determine the chemical composition of exhaust coming out of the SOFC system, to see what byproducts were being produced due to deposition and the chemical reactions at the cell.

The results showed that the SOFC follows similar trends to other research: an initial decline in cell performance as initial siloxanes and carbons are deposited on the surface of the anode, blocking some gas flow rate from occurring. As the deposition process continues, eventually the cell performance stagnates, as fewer sites are available for new deposition to plug. This all occurred relatively quickly compared to other studies, due to the high concentration of siloxane used. At some threshold, the mass transfer became significantly less than the necessary amount to sustain a high current density, resulting in an increasingly quick cell performance failure, as voltage drops to zero as cell resistance spikes. This has not been previously noted for linear siloxanes in an SOFC.

REFERENCES

1. Kaparaju, P.; Rintala, J. Generation of heat and power from biogas for stationary applications: Boilers, gas engines and turbines, combined heat and power (CHP) plants and fuel cells. *Biogas Handb. Sci. Prod. Appl.* **2013**, 404–427, doi:10.1533/9780857097415.3.404.

2. Jaramillo, P.; Matthews, H.S. Landfill-Gas-to-Energy Projects: Analysis of Net Private and Social Benefits. *Environ. Sci. Technol.* **2005**, *39*, 7365–7373, doi:10.1021/es050633j.

3. U.S. Energy Information Adminstration *Heat Content of Natural Gas Consumed*; 2020;

4. Riley, D.M.; Tian, J.; Güngör-Demirci, G.; Phelan, P.; Villalobos, J.R.; Milcarek, R.J. Techno-Economic Assessment of CHP Systems in Wastewater Treatment Plants. *Environ. - MDPI* **2020**, *7*, 1–32, doi:10.3390/environments7100074.

5. Haga, K.; Adachi, S.; Shiratori, Y.; Itoh, K.; Sasaki, K. Poisoning of SOFC anodes by various fuel impurities. *Solid State Ionics* **2008**, *179*, 1427–1431, doi:10.1016/j.ssi.2008.02.062.

6. Andrea, T.; X, C.D.X.; X, M.D.X.; Massimo, D.X.; X, S.D.X. Dealing with fuel contaminants in biogas-fed solid oxide fuel cell (SOFC) and molten carbonate fuel cell (MCFC) plants : Degradation of catalytic and electro-catalytic active surfaces and related gas puri fi cation methods. *Prog. Energy Combust. Sci.* **2017**, *61*, 150–188, doi:10.1016/j.pecs.2017.04.002.

7. Madi, H.; Lanzini, A.; Diethelm, S.; Papurello, D.; Van Herle, J.; Lualdi, M.; Gutzon Larsen, J.; Santarelli, M. Solid oxide fuel cell anode degradation by the effect of siloxanes. *J. Power Sources* **2015**, *279*, 460–471, doi:10.1016/j.jpowsour.2015.01.053.

8. Maček, J.; Novosel, B.; Marinšek, M. Ni-YSZ SOFC anodes-Minimization of carbon deposition. *J. Eur. Ceram. Soc.* **2007**, *27*, 487–491, doi:10.1016/j.jeurceramsoc.2006.04.107.

9. Lanzini, A.; Madi, H.; Chiodo, V.; Papurello, D.; Maisano, S.; Santarelli, M.; Van herle, J. Dealing with fuel contaminants in biogas-fed solid oxide fuel cell (SOFC) and molten carbonate fuel cell (MCFC) plants: Degradation of catalytic and electro-catalytic active surfaces and related gas purification methods. *Prog. Energy Combust. Sci.* **2017**, *61*, 150–188, doi:10.1016/j.pecs.2017.04.002.

10. Shirjeel, M.; Lee, S.; Song, R.; Lee, J.; Lim, T.; Park, S. Fundamental mechanisms involved in the degradation of nickel – yttria stabilized zirconia (Ni – YSZ) anode during solid oxide fuel cells operation : A review. *Ceram. Int.* **2016**, *42*, 35–48, doi:10.1016/j.ceramint.2015.09.006.

11. Tian, J.; Milcarek, R.J. Degradation Comparison of Cyclic and Linear Siloxane

Contamination on Solid Oxide Fuel Cells Ni-YSZ Anode. **2021**, *9*, 1–13, doi:10.3389/fenrg.2021.749771.

12. Piechota, G. Siloxanes in biogas: Approaches of sampling procedure and GC-MS method determination. *Molecules* **2021**, *26*, doi:10.3390/molecules26071953.

13. Wang, N.; Tan, L.; Xie, L.; Wang, Y.; Ellis, T. Investigation of volatile methyl siloxanes in biogas and the ambient environment in a landfill. *J. Environ. Sci. (China)* **2020**, *91*, 54–61, doi:10.1016/j.jes.2020.01.005.

14. Haile, S.M. Fuel cell materials and components. *Acta Mater.* **2003**, *51*, 5981–6000, doi:10.1016/j.actamat.2003.08.004.

15. Ormerod, R.M. Solid oxide fuel cells. *Chem. Soc. Rev.* **2003**, *32*, 17–28, doi:10.1039/B105764M.

16. Minh, N.Q. Solid oxide fuel cell technology - Features and applications. *Solid State Ionics* **2004**, *174*, 271–277, doi:10.1016/j.ssi.2004.07.042.

17. Huijsmans, J.P.P.; Van Berkel, F.P.F.; Christie, G.M. Intermediate temperature SOFC - A promise for the 21st century. *J. Power Sources* **1998**, *71*, 107–110, doi:10.1016/S0378-7753(97)02789-4.

18. Huang, K. Solid Oxide Fuel Cells. In *Materials for Fuel Cells*; Woodhead Publishing Series in Electronic and Optical Materials, 2008; pp. 280–343.

19. Li, G.; Gou, Y.; Qiao, J.; Sun, W.; Wang, Z.; Sun, K. Recent progress of tubular solid oxide fuel cell: From materials to applications. *J. Power Sources* **2020**, *477*, 228693, doi:10.1016/j.jpowsour.2020.228693.

20. Sammes, N.M.; Du, Y.; Bove, R. Design and fabrication of a 100 W anode supported micro-tubular SOFC stack. *J. Power Sources* **2005**, *145*, 428–434, doi:10.1016/j.jpowsour.2005.01.079.

21. Ferraris, M.; De la Pierre, S.; Sabato, A.G.; Smeacetto, F.; Javed, H.; Walter, C.; Malzbender, J. Torsional shear strength behavior of advanced glass-ceramic sealants for SOFC/SOEC applications. *J. Eur. Ceram. Soc.* **2020**, *40*, 4067–4075, doi:10.1016/j.jeurceramsoc.2020.04.034.

22. Gross-Barsnick, S.M. Interaction of glass-ceramic sealants with solid oxide fuel cell components: Thermo-mechanical analysis. In *Intermediate Temperature Solid Oxide Fuel Cells: Electrolytes, Electrodes and Interconnects*; INC, 2019; pp. 411–426 ISBN 9780128174456.

23. Krainova, D.A.; Saetova, N.S.; Farlenkov, A.S.; Khodimchuk, A. V.; Polyakova, I.G.; Kuzmin, A. V. Long-term stability of SOFC glass sealant under oxidising and reducing atmospheres. *Ceram. Int.* **2021**, *47*, 8973–8979, doi:10.1016/j.ceramint.2020.12.019.

24. Anjana, P.S.; Salinigopal, M.S.; Gopakumar, N. Glasses and glass-ceramics as

sealants in solid oxide fuel cell applications. In *Energy Materials: Fundamentals to Applications*; Elsevier Ltd, 2021; pp. 373–404 ISBN 9780128237106.

25. Ding, G.; Gan, T.; Yu, J.; Li, P.; Yao, X.; Hou, N.; Fan, L.; Zhao, Y.; Li, Y. Carbon-resistant Ni1-xCox-Ce0.8Sm0.2O1.9 anode for solid oxide fuel cells fed with methanol. *Catal. Today* **2017**, *298*, 250–257, doi:10.1016/j.cattod.2017.03.060.

26. Li, P.; Wang, R.; Yan, F. Effect of Pr addition into Ni based anode on direct methanol fueled solid oxide fuel cell. *J. Electroanal. Chem.* **2020**, *859*, 113846, doi:10.1016/j.jelechem.2020.113846.

27. Zhang, J.; Zhang, H.; Wu, J.; Zhang, J. Fuel Cell Open Circuit Voltage. *Pem Fuel Cell Test. Diagnosis* **2013**, 187–200, doi:10.1016/b978-0-444-53688-4.00007-3.

28. Milcarek, R.J.; Garrett, M.J.; Welles, T.S.; Ahn, J. Performance investigation of a micro-tubular flame-assisted fuel cell stack with 3,000 rapid thermal cycles. *J. Power Sources* **2018**, *394*, 86–93, doi:10.1016/j.jpowsour.2018.05.060.

29. Huang, Q.A.; Liu, M.; Liu, M. Impedance Spectroscopy Study of an SDC-based SOFC with High Open Circuit Voltage. *Electrochim. Acta* **2015**, *177*, 227–236, doi:10.1016/j.electacta.2014.11.065.

30. Jensen, S.H.; Langnickel, H.; Hintzen, N.; Chen, M.; Sun, X.; Hauch, A.; Butera, G.; Clausen, L.R. Reversible operation of a pressurized solid oxide cell stack using carbonaceous gases. *J. Energy Storage* **2019**, *22*, 106–115, doi:10.1016/j.est.2019.02.003.

31. Bezmalinovic, D.; Simic, B.; Barbir, F. Characterization of PEM fuel cell degradation by polarization change curves. *J. Power Sources* **2015**, *294*, 82–87, doi:10.1016/j.jpowsour.2015.06.047.

32. Gebregergis, A.; Pillay, P.; Bhattacharyya, D.; Rengaswemy, R. Solid Oxide Fuel Cell Modeling. *IEEE Trans. Ind. Electron.* **2009**, *56*, 139–148, doi:10.1109/TIE.2008.2009516.

33. Winterbone, D.E.; Turan, A. Chapter 21 - Fuel Cells. In *Advanced Thermodynamics for Engineers (Second Edition)*; 2015; Vol. 1, pp. 497–526 ISBN 9780444633736.

34. Crowell, L.L.; Yakisich, J.S.; Aufderheide, B.; Adams, T.N.G. Electrical impedance spectroscopy for monitoring chemoresistance of cancer cells. *Micromachines* **2020**, *11*, doi:10.3390/mi11090832.

35. Dean, D.A.; Ramanathan, T.; Machado, D.; Sundararajan, R. Electrical impedance spectroscopy study of biological tissues. *J. Electrostat.* **2008**, *66*, 165–177, doi:10.1016/j.elstat.2007.11.005.

36. Kyle, A.H.; Chan, C.T.O.; Minchinton, A.I. Characterization of three-dimensional tissue cultures using electrical impedance spectroscopy. *Biophys. J.* **1999**, *76*,

2640–2648, doi:10.1016/S0006-3495(99)77416-3.

37. Barfod, R.; Mogensen, M.; Klemensø, T.; Hagen, A.; Liu, Y.-L.; Vang Hendriksen, P. Detailed Characterization of Anode-Supported SOFCs by Impedance Spectroscopy. *J. Electrochem. Soc.* **2007**, *154*, B371–B378, doi:10.1149/1.2433311.

38. Khan, S.; Aijaz Rizvi, S.M.; Urooj, S. Equivalent circuit modelling using electrochemical impedance spectroscopy for different materials of SOFC. In Proceedings of the 2016 3rd International Conference on Computing for Sustainable Global Development (INDIACom); 2016; pp. 1563–1567.

39. Makharia, R.; Mathias, M.F.; Baker, D.R. Measurement of Catalyst Layer Electrolyte Resistance in PEFCs Using Electrochemical Impedance Spectroscopy. *J. Electrochem. Soc.* **2005**, *152*, A970–A977, doi:10.1149/1.1888367.

40. Hsieh, Y.D.; Chan, Y.H.; Shy, S.S. Effects of pressurization and temperature on power generating characteristics and impedances of anode-supported and electrolyte-supported planar solid oxide fuel cells. *J. Power Sources* **2015**, *299*, 1–10, doi:10.1016/j.jpowsour.2015.08.080.

41. Nielsen, J.; Mogensen, M. SOFC LSM:YSZ cathode degradation induced by moisture: An impedance spectroscopy study. *Solid State Ionics* **2011**, *189*, 74–81, doi:10.1016/j.ssi.2011.02.019.

42. Milcarek, R.J.; Garrett, M.J.; Ahn, J. Micro-tubular flame-assisted fuel cell stacks. *Int. J. Hydrogen Energy* **2016**, *41*, 21489–21496, doi:10.1016/j.ijhydene.2016.09.005.

43. Tian, J.; Milcarek, R.J. Siloxane Deposition on the Ni-YSZ Solid Oxide Fuel Cell Anode Exposed to Bio-Syngas. *J. Electrochem. Soc.* **2021**, *168*, 044503, doi:10.1149/1945-7111/abf21a.

44. Bartle, K.D.; Myers, P. History of gas chromatography. *TrAC Trends Anal. Chem.* **2002**, *21*, 547–557, doi:10.1016/S0165-9936(02)00806-3.

45. McNair, H.M.; Miller, J.M.; Snow, N.H. *Basic gas chromatography*; John Wiley and Sons, 2019;

46. McWilliam, I.; Dewar, R. Flame ionization detector for gas chromatography. *Nature* **1958**, *181*, 760.

47. Parry V, K.D. Scanning Electron Microscopy : An introduction. *III-Vs Rev.* **2000**, *13*, 40–44.

48. Zhou, W.; Apkarian, R.P.; Wang, Z.L.; Joy, D. Fundamentals of Scanning Electron Microscopy 2006, 1–40.

49. Madi, H.; Diethelm, S.; Poitel, S.; Ludwig, C.; Van herle, J. Damage of Siloxanes on Ni-YSZ Anode Supported SOFC Operated on Hydrogen and Bio-Syngas. *Fuel*

Cells **2015**, *15*, 718–727, doi:10.1002/fuce.201400185.

50. Tian, J.; Milcarek, R.J. Investigating the degradation mechanism of the solid oxide fuel cell nickel-yttria stabilized zirconia anode under siloxane contamination. *J. Power Sources* **2020**, *480*, 229122, doi:10.1016/j.jpowsour.2020.229122.

51. Dewil, R.; Appels, L.; Baeyens, J. Energy use of biogas hampered by the presence of siloxanes. *Energy Convers. Manag.* **2006**, *47*, 1711–1722, doi:10.1016/j.enconman.2005.10.016.

52. Boonme, P.; Pakpayat, N.; Yotmanee, K.; Kunlawijitrungsee, S.; Maneenuan, D. Evaluation of Shampoos Containing Silicone Quaternary Microemulsion. *J. Appl. Pharm. Sci.* **2011**, *1*, 59–63.

53. Martin, F.L.; Ames, J.M. Comparison of Flavor Compounds of Potato Chips Fried in Palmolein and Silicone Fluid. *J. Am. Oil Chem.* **2001**, *78*, 863.

54. Parker, M.H.; Cameron, S.M.; Hughbanks, J.C.; Reid, D.E. Comparison of occlusal contacts in maximum intercuspation for two impression techniques. *J. Prosthet. Dent.* **1997**, *78*, 255–259, doi:10.1016/S0022-3913(97)70023-4.

55. Liu, N.; Shi, Y.; Li, W.; Xu, L.; Cai, Y. Concentrations and distribution of synthetic musks and siloxanes in sewage sludge of wastewater treatment plants in china. *Sci. Total Environ.* **2014**, *476–477*, 65–72, doi:10.1016/j.scitotenv.2013.12.124.

56. Cortada, C.; Dos Reis, L.C.; Vidal, L.; Llorca, J.; Canals, A. Determination of cyclic and linear siloxanes in wastewater samples by ultrasound-assisted dispersive liquid-liquid microextraction followed by gas chromatography-mass spectrometry. *Talanta* **2014**, *120*, 191–197, doi:10.1016/j.talanta.2013.11.042.

57. Silva, E.N.; Cantillo-Castrillon, M.; Dantas, T.M.; Mesquita, Y.M.; Maia, D.A.S.; Bastos-Neto, M.; Barcellos, W.M.; Azevedo, D.C.S. Siloxane adsorption by porous silica synthesized from residual sand of wastewater treatment. *J. Environ. Chem. Eng.* **2021**, *9*, doi:10.1016/j.jece.2020.104805.

58. Tran, T.M.; Kannan, K. Occurrence of cyclic and linear siloxanes in indoor air from Albany, New York, USA, and its implications for inhalation exposure. *Sci. Total Environ.* **2015**, *511*, 138–144, doi:10.1016/j.scitotenv.2014.12.022.

59. Wang, X.M.; Lee, S.C.; Sheng, G.Y.; Chan, L.Y.; Fu, J.M.; Li, X.D.; Min, Y.S.; Chan, C.Y. Cyclic organosilicon compounds in ambient air in Guangzhou, Macau and Nanhai, Pearl River Delta. *Appl. Geochemistry* **2001**, *16*, 1447–1454, doi:10.1016/S0883-2927(01)00044-0.

60. Beylot, A.; Villeneuve, J.; Bellenfant, G. Life Cycle Assessment of landfill biogas management : Sensitivity to diffuse and combustion air emissions. *Waste Manag.* **2013**, *33*, 401–411, doi:10.1016/j.wasman.2012.08.017.

61. Kapoor, R.; Ghosh, P.; Tyagi, B.; Vijay, V.K.; Vijay, V.; Thakur, I.S.; Kamyab,

H.; Nguyen, D.D.; Kumar, A. Advances in biogas valorization and utilization systems: A comprehensive review. *J. Clean. Prod.* **2020**, *273*, 123052, doi:10.1016/j.jclepro.2020.123052.

62. Stanuch, I.; Sozańska, M.; Biegańska, J.; Cebula, J.; Nowak, J. Fluctuations of the elemental composition in the layers of mineral deposits formed on the elements of biogas engines. *Sci. Rep.* **2020**, *10*, 4244, doi:10.1038/s41598-020-61212-x.

63. Lu, Y.; Yuan, T.; Wang, W.; Kannan, K. Concentrations and assessment of exposure to siloxanes and synthetic musks in personal care products from China. *Environ. Pollut.* **2011**, *159*, 3522–3528, doi:10.1016/j.envpol.2011.08.015.

64. Papurello, D.; Lanzini, A. SOFC single cells fed by biogas : Experimental tests with trace contaminants. *Waste Manag.* **2018**, *72*, 306–312, doi:10.1016/j.wasman.2017.11.030.

65. Escudero, M.J.; Maffiotte, C.A.; Serrano, J.L. Long-term operation of a solid oxide fuel cell with MoNi – CeO 2 as anode directly fed by biogas containing simultaneously sulphur and siloxane. *J. Power Sources* **2021**, *481*, 229048, doi:10.1016/j.jpowsour.2020.229048.

66. Läntelä, J.; Rasi, S.; Lehtinen, J.; Rintala, J. Landfill gas upgrading with pilot-scale water scrubber: Performance assessment with absorption water recycling. *Appl. Energy* **2012**, *92*, 307–314, doi:10.1016/j.apenergy.2011.10.011.

67. Raich-Montiu, J.; Ribas-Font, C.; de Arespacochaga, N.; Roig-Torres, E.; Broto-Puig, F.; Crest, M.; Bouchy, L.; Cortina, J.L. Analytical methodology for sampling and analysing eight siloxanes and trimethylsilanol in biogas from different wastewater treatment plants in europe. *Anal. Chim. Acta* **2014**, *812*, 83–91, doi:10.1016/j.aca.2013.12.027.

68. Hagmann, M.; Heimbrand, E.; Hentschel, P. Determination of siloxanes in biogas from landfills and sewage treatment plants. In Proceedings of the Proceedings Sardinia 99, seventh international waste management and landfill symposium; Cagliari, Italy, 1999.

69. Kikuchi, Y.; Matsuda, J.; Tachikawa, Y.; Shiratori, Y.; Taniguchi, S.; Sasaki, K. Degradation iof SOFCs by Various Impurities: Impedance Spectroscopy and Microstructural Analysis. *ECS Trans.* **2017**, *78*, 1253–1260, doi:10.1149/07801.1253ecst.

70. Brus, G.; Komatsu, Y.; Kimijima, S.; Szmyd, J.S. An Analysis of Biogas Reforming Process on Ni/YSZ and Ni/SDC Catalysts. *Int. J. Thermodyn.* **2012**, *15*, 43–51, doi:10.5541/ijot.315.

71. Watanabe, M.; Uchida, H.; Yoshida, M. Effect of Ionic Conductivity of Zirconia Electrolytes on the Polarization Behavior of Ceria-Based Anodes in Solid Oxide Fuel Cells. *J. Electrochem. Soc.* **1997**, *144*, 1739.

72. Ametek EnergyLab Apps-XM Series 2016.

73. Radenahmad, N.; Azad, A.T.; Saghir, M.; Taweekun, J.; Bakar, M.S.A.; Reza, M.S.; Azad, A.K. A review on biomass derived syngas for SOFC based combined heat and power application. *Renew. Sustain. Energy Rev.* **2020**, *119*, 109560, doi:10.1016/j.rser.2019.109560.

74. Tansel, B.; Surita, S.C. Differences in volatile methyl siloxane (VMS) profiles in biogas from landfills and anaerobic digesters and energetics of VMS transformations. *Waste Manag.* **2014**, *34*, 2271–2277, doi:10.1016/j.wasman.2014.07.025.

APPENDIX A

COPYRIGHT APPROVALS FOR IMAGES USED

Figure 1: Solid Oxide Fuel Cell Schematic

This Agreement between School for Engineering of Matter, Transport, and Energy -- Derall Riley ("You") and Elsevier ("Elsevier") consists of your license details and the terms and conditions provided by Elsevier and Copyright Clearance Center.

License Number	5176281274120
License date	Oct 26, 2021
Licensed Content Publisher	Elsevier
Licensed Content Publication	Acta Materialia
Licensed Content Title	Fuel cell materials and components☆ ☆ ☆ The Golden Jubilee Issue—Selected topics in Materials Science and Engineering: Past, Present and Future, edited by S. Suresh.
Licensed Content Author	Sossina M Haile
Licensed Content Date	Nov 25, 2003
Licensed Content Volume	51
Licensed Content Issue	19
Licensed Content Pages	20

Start Page	5981
End Page	6000
Type of Use	reuse in a thesis/dissertation
Portion	figures/tables/illustrations
Number of figures/tables /illustrations	1
Format	electronic
Are you the author of this Elsevier article?	No
Will you be translating?	No
Title	Fabrication of Solid Oxide Fuel Cells and the Effects of Linear Siloxane Deposition on Cell Performance
Institution name	Arizona State University
Expected presentation date	Dec 2021
Portions	Figure 1
Requestor Location	School for Engineering of Matter, Transport, and Energy 501 E Tyler Mall PO Box 876106 TEMPE, AZ 85287 United States Attn: School for Engineering of Matter, Transport, and Energy
Publisher Tax ID	98-0397604

Figure 2: Polarization Curve Example

License Number	5176331203685
License date	Oct 26, 2021
Licensed Content Publisher	Elsevier
Licensed Content Publication	Elsevier Books
Licensed Content Title	Advanced Thermodynamics for Engineers
Licensed Content Author	Desmond E. Winterbone,Ali Turan
Licensed Content Date	Jan 1, 2015
Licensed Content Pages	30
Start Page	497
End Page	526
Type of Use	reuse in a thesis/dissertation
Portion	figures/tables/illustrations

Number of figures/tables /illustrations	1
Format	electronic
Are you the author of this Elsevier chapter?	No
Will you be translating?	No
Title	Fabrication of Solid Oxide Fuel Cells and the Effects of Linear Siloxane Deposition on Cell Performance
Institution name	Arizona State University
Expected presentation date	Dec 2021
Portions	Figure 21.10
Requestor Location	School for Engineering of Matter, Transport, and Energy 501 E Tyler Mall PO Box 876106 TEMPE, AZ 85287 United States Attn: School for Engineering of Matter, Transport, and Energy
Publisher Tax ID	98-0397604

Figure 6: Example Gas Chromatography Schematic

License Number	5176290096621
License date	Oct 26, 2021
Licensed Content Publisher	Elsevier
Licensed Content Publication	TrAC Trends in Analytical Chemistry
Licensed Content Title	History of gas chromatography
Licensed Content Author	Keith D. Bartle,Peter Myers
Licensed Content Date	Sep 10, 2002
Licensed Content Volume	21
Licensed Content Issue	9-10
Licensed Content Pages	11
Start Page	547
End Page	557

Type of Use	reuse in a thesis/dissertation
Portion	figures/tables/illustrations
Number of figures/tables /illustrations	1
Format	electronic
Are you the author of this Elsevier article?	No
Will you be translating?	No
Title	Fabrication of Solid Oxide Fuel Cells and the Effects of Linear Siloxane Deposition on Cell Performance
Institution name	Arizona State University
Expected presentation date	Dec 2021
Portions	Figure 2
Requestor Location	School for Engineering of Matter, Transport, and Energy 501 E Tyler Mall PO Box 876106 TEMPE, AZ 85287 United States Attn: School for Engineering of Matter, Transport, and Energy
Publisher Tax ID	98-0397604

Figure 7: Examples of Linear and Cyclic Siloxanes

License Number	5176290343617
License date	Oct 26, 2021
Licensed Content Publisher	Elsevier
Licensed Content Publication	Energy Conversion and Management
Licensed Content Title	Energy use of biogas hampered by the presence of siloxanes
Licensed Content Author	Raf Dewil,Lise Appels,Jan Baeyens
Licensed Content Date	Aug 1, 2006
Licensed Content Volume	47
Licensed Content Issue	13-14
Licensed Content Pages	12
Start Page	1711
End Page	1722

Type of Use	reuse in a thesis/dissertation
Portion	figures/tables/illustrations
Number of figures/tables /illustrations	1
Format	electronic
Are you the author of this Elsevier article?	No
Will you be translating?	No
Title	Fabrication of Solid Oxide Fuel Cells and the Effects of Linear Siloxane Deposition on Cell Performance
Institution name	Arizona State University
Expected presentation date	Dec 2021
Portions	Figure 2
Requestor Location	School for Engineering of Matter, Transport, and Energy 501 E Tyler Mall PO Box 876106 TEMPE, AZ 85287 United States Attn: School for Engineering of Matter, Transport, and Energy
Publisher Tax ID	98-0397604